Report on the theme
"Modern Trends and Developments in Raman Microspectroscopy and Photoluminescence for Condensed Matter Studies" for the years 2018-2020

Theme code: 04-4-1133-2018/2020
Laboratory: Frank Laboratory of Neutron Physics
Department: Sector of Raman spectroscopy
Theme leaders: G.M. Arzumanyan, N. Kučerka

CONTENT

Activities in 2018-2020 were implemented in accordance with the research programme and the main tasks listed within the theme "Modern Trends and Developments in Raman Microspectroscopy and Photoluminescence for Condensed Matter Studies" included into the JINR Topical Plan.

1. Introduction to spontaneous and enhanced Raman spectroscopy

Raman spectroscopy is a spectroscopic technique used in condensed matter physics and chemistry to study vibrational, rotational, and other low-frequency modes in a system. It depends on the inelastic scattering, or Raman scattering of monochromatic light, usually from a laser in the visible, near-infrared or near-ultraviolet range of electromagnetic spectra.

Over the many years Raman spectroscopy has been recognized to be a powerful tool for various applications, including bioanalytical and biomedical ones. It's well-known that Raman spectra probe molecular vibrations that provide a highly specific fingerprint of the molecular structure and biochemical composition of tissues without external markers. In principle, diseases and other pathological anomalies lead to chemical and structural changes on the molecular level which also alert the vibrational spectra and which can be used as sensitive, phenotypic markers of the disease. As these spectral changes are very specific and unique, they are also called fingerprint. The advantages of the methods include that they are non-destructive and do not require extrinsic contrast-enhancing agents.

On the other hand, this technique has a major drawback that is a low sensitivity, which limits its practical application. The reason for this lack is that only one Raman photon out of 10^6–10^8 photons of incident light can be scattered. However, there are an effective ways developed to solve this problem like SERS (Surface-Enhanced Raman Spectroscopy), CARS (Coherent Antistokes Raman Spectroscopy), their combination – SECARS (Surface-Enhanced CARS), SRS (Stimulated Raman Scattering), TERS (Tip-Enhanced raman spectroscopy), etc.

Activities in the years of 2018-2020 were mainly focused on the further development of SERS and CARS towards higher levels of sensitivity and imaging contrast, and eventually bringing them together as a modern and insufficiently explored spectroscopic tool.

2. Research activities in 2018-2020

<u>Expected main results upon the theme completion:</u>

- **Completion of the upgraded optical platform development for ultrasensitive spectroscopy SECARS.**
- **Selection of the most optimal and effective SERS-active substrates for a surface-enhanced raman spectroscopy.**
- **Systematic experiments on SECARS spectroscopy and intensity mapping with picosecond laser pulses.**
- **Detection of extremely low concentrations of organic molecules with the use of SERS and SECARS**
- **Synthesis and study of the spectral and structural characteristics of "core-shell" up-conversion phosphors with various rare earth elements located in their core and tests in biomedical application.**
- **Realization of a contrast and selective imaging of model samples by Raman microscopy and up-conversion luminescence.**

2.1 SERS spectroscopy

2.1.1. Tests of various configuration of SERS-active substrates with a purpose of an optimal selection for the effective enhanced spectroscopy.

Surface-Enhanced Raman Spectroscopy is an analytical method in biomedicine, environmental monitoring, forensic science and many other areas of human activity, which allows to obtain an information about various compounds at very low concentrations. The high sensitivity of this method is ensured by the use of nanostructured metal surfaces to adsorb the analyzed molecules, the so-called SERS active substrates. SERS activity strongly depends on the nature of metal and surface roughness. Therefore, SERS active substrate fabrication is a very important field in SERS research. The two most common SERS active substrates are metal colloids of coinage metals of Au, Ag and Cu obtained from chemical reduction, and the metal electrode surfaces roughened by one or more electrochemical oxidation–reduction cycles. The recent advancement of nanotechnology has been utilized to fabricate various nanostructures from nanoparticles to nanowires, which can be used as SERS active substrates.

During 2018-2019 a large number of various configuration of SERS-active substrates were probed. In particular, we used substrates developed and constructed in Belarus Republic (BelSERS), Lithuania (ATO ID), Australia (Flew Solutions), Russia (ITAE RAS, Moscow) and some others. When choosing substrates, we proceeded primarily from their plasmonic-spectral characteristics, adapted to the near-IR region. This, in turn, was due to the fact that lasers in the IR range are used to generate CARS signal at our Raman microspectrometer.

Main characteristics of the probed SERS active substrates:

1. ***<u>"BelSERS" substrates (Fig.1), Belarus, BSUIR</u>***
   - **substrate material**: glass slide with SERS-active zone (35 or 50 mm^2) composed of Ag or Au stochastic nanoparticles or dendrites
   - **detection limit**: 10^{-3} – 10^{-13} M
   - **excitation wavelengths**: visible, IR
   - **sampling methods**: drop deposition or immersion
   - **shelf time:** 6 months
   - **store in:** vacuum, air

Fig. 1. "BelSERS" substrates – general view

2. ***<u>"MATO & RANDA" substrates (Fig.2), Lithuania, ATO ID</u>***
   - **substrate material**: soda-lime glass slide with 5x5 mm active zone: Au for MATO and Ag for RANDA
   - **detection limit**: 10^{-2} – $10^{(-10-12)}$ M
   - **excitation wavelengths**: 600nm to NIR (MATO), 440nm to NIR (RANDA)

- **shelf time:** 2 months
- **store in:** vacuum

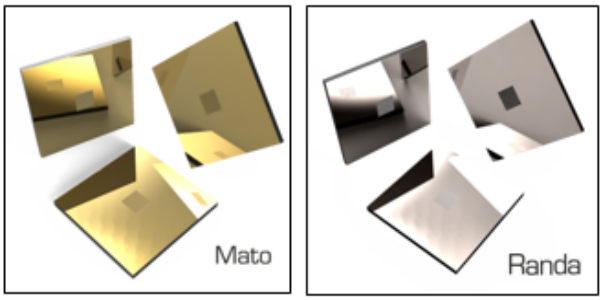

Fig. 2. "MATO" and "RANDA" SERS-substrates

3. ***"FLEW SERS" substrates (Fig.3), Australia, FLEW Solution***
   - **substrate material**: glass slides with SERS-active zone (12.6 mm^2) composed of nanostructured Cu (Cuo) and coated with Au
   - **detection limit**: ppm/micromolar (μM)
   - **excitation wavelengths (recommended)**: 785 nm
   - **sampling methods**: drop deposition or immersion
   - **shelf time:** 6 months
   - **store in: nitrogen, vacuum, air**

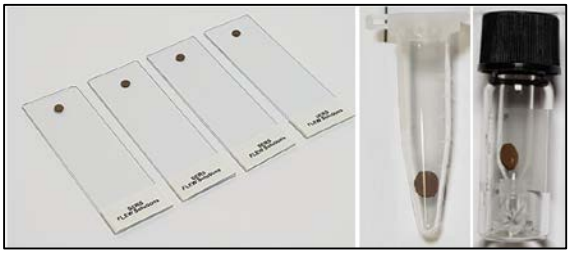

Fig. 3. FLEW SERS-substrates

The comparative SERS-measurement results are demonstrated in Fig.4 (excitation 633 nm) and Fig.5 (excitation 785 nm). As for model analyte DTNB acid molecules were exploit at different concentrations.

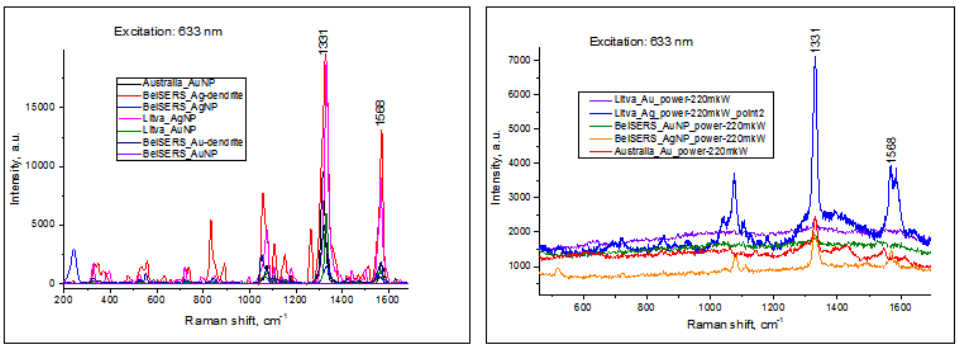

Fig. 4. SERS spectra of DTNB at the concentrations of 10^{-5}M (left) and 10^{-10}M (right), exc. 633 nm

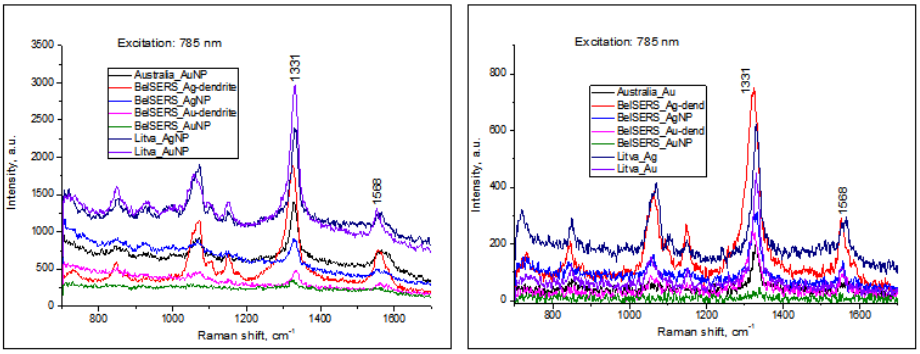

Fig. 5. SERS spectra of DTNB at the concentrations of 10^{-5}M (left) and 10^{-8}M (right), exc. 785 nm

It is clearly seen from the demonstrated Raman spectra that the BelSERS and ATO ID SERS-substrates shows better sensitivity in comparison with the Australian one. Also, it should be noted, that despite the fact, that all of these substrates are targeted at IR SERS, the highest sensitivity was detected at the excitation of 633 nm. Briefly summarizing this chapter it is worth to mention that the gained experience in probing various SERS-substrates was an important step towards SECARS experiments.

2.1.2 Highly sensitive detection of Raman spectra of organic molecules (single units) using dendridic Ag nanostructures.

The development of modern biosensing techniques to overcome the problem of reliable detection, identification, and structural study of diverse bioorganic molecules at ultralow concentrations is still an urgent objective of specialists in many spheres including medicine, biology, forensics, ecology, pharmaceutics and so on. In 2019 we used so-called Ag corrosive deposition on a macroporous silicon (macro-PSi) template to grow 3D silver dendritic structure that demonstrate an unprecedented sensitivity in SERS spectroscopy.

Fig. 6 shows SEM images of the surface and the cross-sections of the mono-Si and macro-PS samples that were processed in the solution of $AgNO_3$ salt for 3 minutes. Considering the Ag deposition on the surface of mono-Si subjected to ion etching we see an Ag layer, which consists of Ag NPs of different diameters and Ag dendrites (Fig.3 a,c). Most of the Ag NPs has an average diameter of 100 nm, but there are also particles of large diameter varying from 500 to 2000 nm. A thickness of the Ag layer is 300-500 nm and the Ag particles have a shape of a slightly flattened ball. It is important to note that Ag dendrites on mono-Si have a much less developed structure compared to Ag dendrites on macro-PS, and moreover, it is difficult to distinguish the Ag particles from which they consist.

As seen from Fig.6 (b,d), a developed network of the Ag NPs and Ag dendrites is formed on the surface of the macro-PS. It is hard to correctly evaluate a density of the Ag NPs formed at the surface of the Si skeleton since they are covered by dendrites. A thickness of the dendritic layer is rather uniform (3-3.5 μm). As can be seen from the sample cross-section (Fig.6 d), an external surface of the macro-PS is rough and the Ag NPs and Ag dendrites are formed on it. The dendrites are directed both vertically and laterally along the surface of the macro-PS. A length of central trunks of the lateral dendrites reaches 20-25 μm, and the lateral branches – about 3-7 microns (Fig.6 b). There is a large number of additional sprouts of 100-300 nm length on the lateral branches of the dendrites. The structure of the dendrites is very rich and all their elements (central trunk and lateral branches) consist of well distinguishable Ag NPs. Moreover, it is clearly seen from Fig.6 d, that Ag dendrites are formed

on the sharp parts of the rough surface of the Si skeleton. Advantageously, the dendrites are formed at the periphery of the pore entrances and their number for a single pore is about 9-12 pieces. Some of the dendrites are located almost vertically and they have a short length of 1.0 - 2.5 μm.

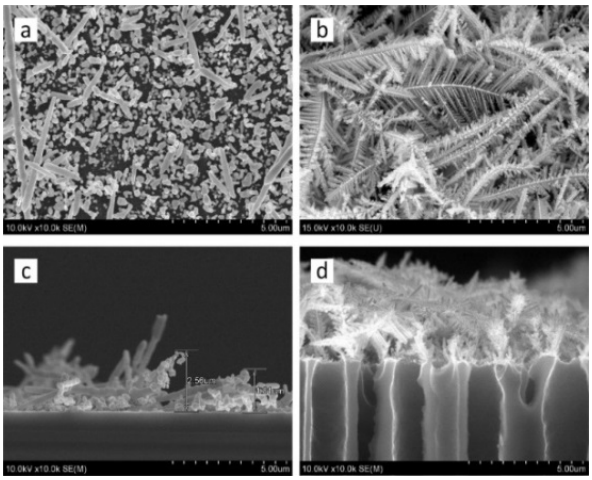

Fig. 6. SEM images of (a, b) top and (c, d) cross-section views of (a, c) mono-Si and (b, d) macro-PS with a deposited Ag layer.

The better understanding of the morphology effect on the SERS measurements can be given by a computer simulation of an electric field in the silver structures on mono- and macro-PSi. Figure 7 shows examples of the area selected for the simulation of the electric field in dendrites.

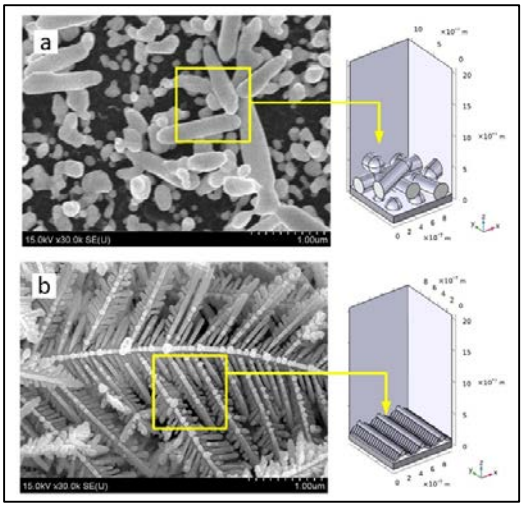

Fig. 7. Areas selected for the simulation of the electric field strength in the silver dendrites on (a) mono-Si and (b) macro-PSi.

Figure 8 shows the results of simulations performed for the fabricated and experimentally studied Ag dendrites based on mono- and macro-PS. Simulations showed that the maximum electric field strength is in the mono-Si based dendrite silver structure. However, there are only a few such hot spots with a large field enhancement. Therefore, a molecule of interest in dilute solutions will interact with such hotspots on a rare occasion. On the other hand PS-based silver dendrite structures have evenly distributed areas with an electric field enhancement. This electric field has a lower strength, but due to a larger effective area, the probability of detection and hence a general signal will be better from such structures than from dendrites on mono-Si.

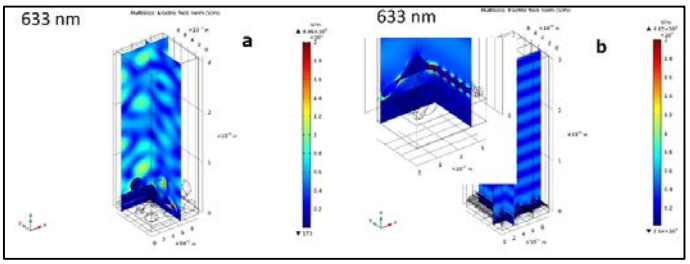

Fig. 8. Electric field strength distribution simulated for the silver dendrites on (a) mono-Si and (d) macro-PS

As for the SERS measurements we selected 4-MBA as a substance for analysis because this analyte is characterized smaller Raman cross section comparing with organic dyes that are more often used to estimate a SERS-activity. Fig. 9 shows the SERS spectra of the 4-MBA molecules deposited on Ag nanostructures on mono-Si and macro-PS substrates. The analyte was adsorbed during immersion of the substrates in the 4-MBA solution of with a concentration of 10-6 M for 1 h, followed by drying at room temperature. The excitation was carried out by laser radiation at wavelengths of 633 nm and 785 nm.

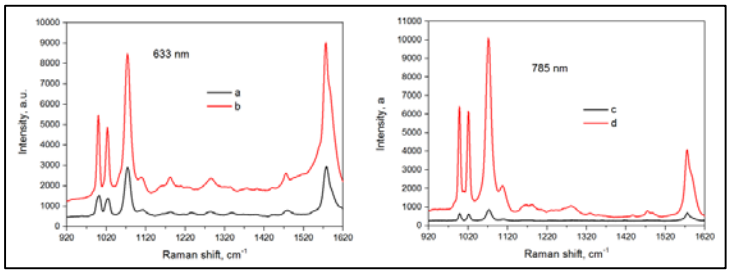

Fig. 9. SERS spectra of the 4-MBA molecules with a concentration of 10^{-6} M, obtained on the surface of the Ag layers on (a, c) mono-Si and (b, d) macro-PS, excited by 633 and 785 nm lasers.

Next, we revealed the minimal concentration of the 4-MBA solution at which its molecules are still detected after adsorption on the silvered macro-PS. Figure 10 presents the SERS spectra of 4-MBA at 10^{-6} to 10^{-16} M concentrations, which were obtained by the collection and integration of three SERS spectra maps at 633 nm excitation wavelength. We scanned a 100 × 100 μm area for each map with a step of 10 μm. Each point of the maps was excited for 1s. All the informative SERS spectra are characterized by the presence of the 4-MBA bands. The SERS spectrum of 4-MBA adsorbed from 10^{-6} M is the strongest one. The decrease of the concentration down to 10^{-16} M led to gradual lowering the SERS signal but the bands at 988, 1021, 1075 and 1573 cm^{-1} are still remaining distinguished.

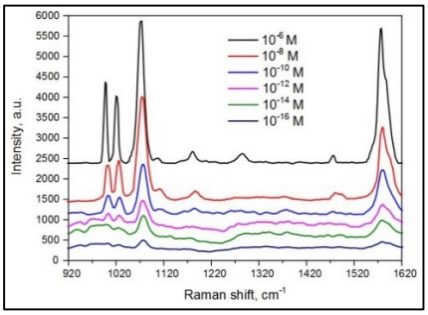

Fig. 10. Average SERS spectra of three maps of the Ag-dendrites/macro-PS kept in the 4-MBA solutions with different concentrations. The excitation wavelength is 633 nm

Summarizing this part of the report its worth to note the following: 3D silver nanostructures, which consist of Ag NPs and network of Ag dendrites deposited on the surface of macro-PS, are fabricated and investigated. With the use of such substrates it was possible for the first time to detect 4-MBA molecules with very low concentrations of 10^{-16} M.

We also registered SERS spectra of the human lactoferrin molecules adsorbed on a silvered porous silicon (por-Si) from 10^{-6}–10^{-18} M solutions. The SERS spectra of lactoferrin adsorbed from 10^{-6} M solution were rather weak but a decrease of the concentration to 10^{-10} M led to an enormous growth of the SERS signal. This effect took place as oligomers of lactoferrin were broken down to monomeric units while its concentration was reduced. Oligomers are too large for a uniform overlap with electromagnetic field from silver particles. They cannot provide an intensive SERS signal from the top part of the molecules in contrast to monomers that can be completely covered by the electromagnetic field. The SERS spectra of lactoferrin at the 10^{-14} and 10^{-16} M concentrations were less intensive and started to change due to increasing contribution from the laser burned molecules. To prevent overheating the analyte molecules were protected with graphene (Fig. 11), which allowed the detection of lactoferrin adsorbed from the 10^{-18} M solution.

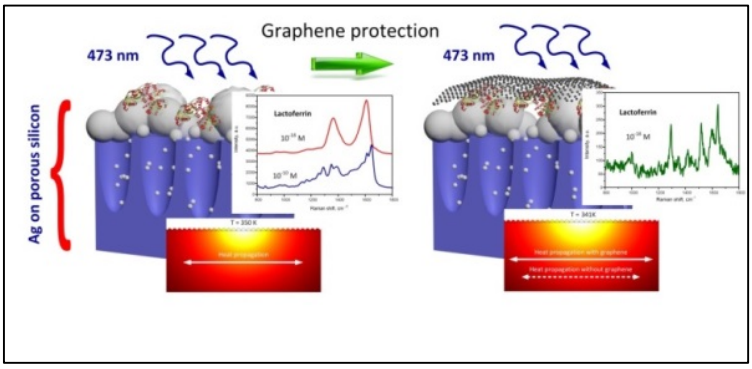

Fig. 11. Schematic of the analyte molecule protection on the silvered por-Si with graphene

The initial SERS-measurement of lactoferrin was devoted to reveal if the silvered por-Si substrate provides the registration of its spectrum free of changes caused by the interaction of the bioorganic molecule with metallic particles and denaturation under laser irradiation. Next, we revealed the minimal concentration of the lactoferrin solution at which its molecules are still detected after adsorption on the silvered por-Si. Figure 12 presents the SERS spectra of lactoferrin at 10^{-6} to 10^{-18} M concentrations, which were obtained by the collection and integration of the SERS spectra maps.

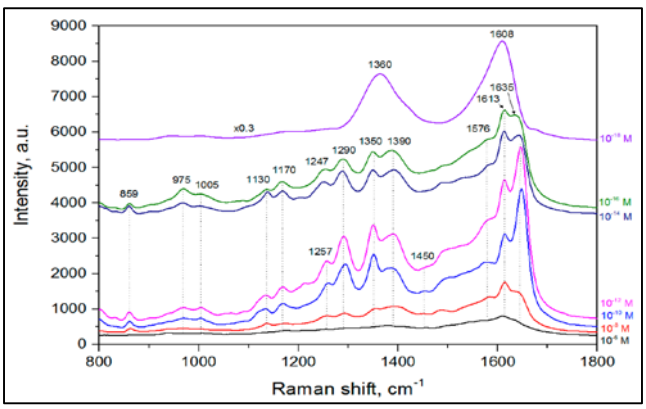

Fig. 12. SERS spectra of lactoferrin molecules adsorbed on the silvered por-Si

We exploit two SERS-active substrates from different batches and scanned a 10x10 μm surface area of both substrates with a step of 1μm. Each point of the maps was excited for 2s. The laser power was decreased to 0.14 mW in contrast to the previous measurement to eliminate a harmful photothermal effect. All the informative SERS spectra are characterized by the presence of this analyte bands.

To overcome the limitation of the 10^{-16} M lactoferrin concentration, at which it can be detected, we used the protection with graphene that was first successfully tested on the R6G molecules. Figure 13 shows the SERS spectrum obtained for the lactoferrin molecules adsorbed from the solution of attomolar concentration on the silvered por-Si and then coated with graphene. We registered spectrum during 2s.

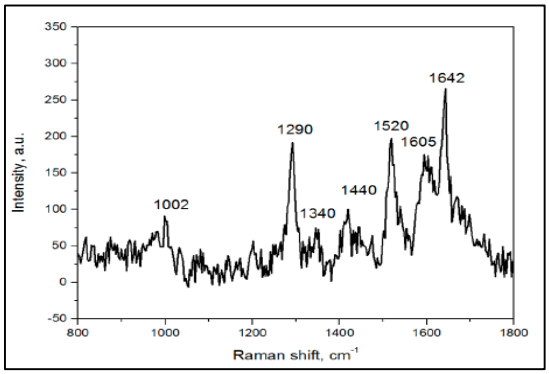

Fig. 13. SERS spectrum of the lactoferrin molecules adsorbed on the silvered por-Si from 10^{-18} M solution and then protected with graphene.

Despite the SERS spectrum intensity being relatively low, most of the lactoferrin Raman bands were presented there: 1002 cm^{-1} (Phe), 1290 cm^{-1} (Amide III), 1340 cm^{-1} (Trp), 1440 cm^{-1} (CH_2), 1605 cm^{-1} (Tyr) and 1642 cm^{-1} (Amide I). **Thus, we demonstrated the ability to measure the SERS spectra of the human lactoferrin molecules adsorbed on the silvered por-Si from the 10^{-6}–10^{-18} M water solutions.**

2.1.3 Upgrade of the "CARS" microspectrometer software

In 2019 we continued our activities to complete the development of “scan-CARS” modality started in 2018 which was based on the following technical assignment:

Module initialization:

a) Set start wavelength - $\lambda_{pump}S$ (dialog box)
b) Set end wavelength - $\lambda_{pump}F$ (dialog box)
c) Set wavelength step (dialog box):
   minimum step of 0.1 nm, maximum step of 1/10 ($\lambda_{pump}F$ - $\lambda_{pump}S$)
d) Control of aaccumulation time of the CARS signal at each spectral point (dialog box)
e) Radio knobs: closing/opening of 2 shutters (Stokes and OPO during the wavelength tuning and temperature stabilization)
f) Prior of sending for run - a warning about the estimated duration of the recording time
g) Formation of a graphical output window of the CARS spectrum in real time - according to the “NanoSP” standards
h) Run for execution

i) Final stage: a dialog box opens - saving/erasing the CARS spectrum. New spectrum/ output.

During 2019 we tested this program product using various samples. As an example, one of the obtained results with polystyrene beads in the range of 1620 – 1540 cm^{-1} is demonstrated in Fig.14.

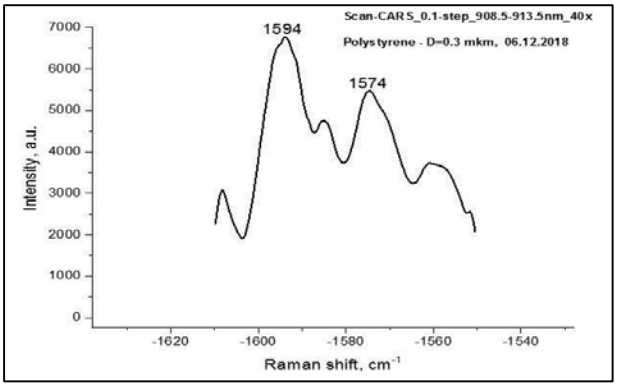

Fig. 14. CARS spectrum of polystyrene beads in the range of 1620 – 1540 cm^{-1}

This modality makes the "CARS" microspectrometer an advanced system for multi-color excitation experiments, such as scanning CARS and others.

2.1.4 SERS vs SECARS spectra and intensity maps of organic Raman-reporter molecules. Realization of highly contrast and selective chemical imaging by SECARS.

Presently, the investigations around SERS are devoted, among other topics, to clarification of physical mechanisms of laser light interaction with SERS-active surfaces and, in particular, of surface-enhanced coherent anti-Stokes Raman scattering (SECARS), as well as to possible applications of SERS in biology, biochemistry and medicine, pharmacy, etc. In 2019-2020, our study was aimed to reveal the possibilities of detecting reproducible SERS and SECARS signals from TNB molecules adsorbed at the Au-NPs/CeO_2 SERS-active surface without destruction of the surface itself or the conjugates.

Laser light, illuminating SERS-active nanostructured CeO_2/Al/Al_2O_3 thin film samples with reporter molecules/Au-NP conjugates on the CeO_2 surface, may cause irreversible modifications of the conjugates and of the surface structure field enhancing properties. As a result, the observed Raman signal decreases or vanishes. In our study the limits of the laser light intensity suitable for nondestructive spectroscopic studies have been assessed using continuous and quasi continuous wave (mode locked ps pulse) laser radiation. This radiation was used as a pump for linear and nonlinear Raman microspectroscopy of reporter molecules adsorbed on the surface of plasmonic substrate. Reducing laser power below certain levels allowed reproducible mapping of surface-enhanced Raman scattering and surface-enhanced coherent anti-Stokes Raman scattering signal strengths at the reporter molecule Raman shifts.

Spectra and microimages of SERA and SECARS radiation were recorded, with a high spatial resolution, using a Confotec CARS confocal microspectrometer, (SOL Instruments Ltd., Belarus). The CARS part of the spectrometer was based on a diode-pumped passively mode-locked laser (1064 nm, 7 ps, 85 MHz, 5 W, ~5–7 cm^{-1} linewidth) and an optical parametric oscillator (OPO) synchronously pumped by the frequency-doubled 1,064-nm radiation. The signal beam of the OPO (690–990 nm, 6 ps, 150–350 mW,) and a part of the 1,064-nm beam, with parallel polarizations, were

collinearly overlapped and employed, respectively, as pump (λ_p) and Stokes (λ_S) radiation in the CARS process to generate narrow lines of the coherent anti-Stokes signals at $\lambda_{aS} = \lambda_p/(2 - \lambda_p/\lambda_S)$. The signals could be detected by the system within the Raman shift range of 990–3,580 cm^{-1}. CARS signals could be detected by either a cooled photomultiplier tube module or a cooled 2,048 × 122 elements CCD array photodetector. Raman spectra were detected by the same CCD detector (optical schematic in Fig.15).

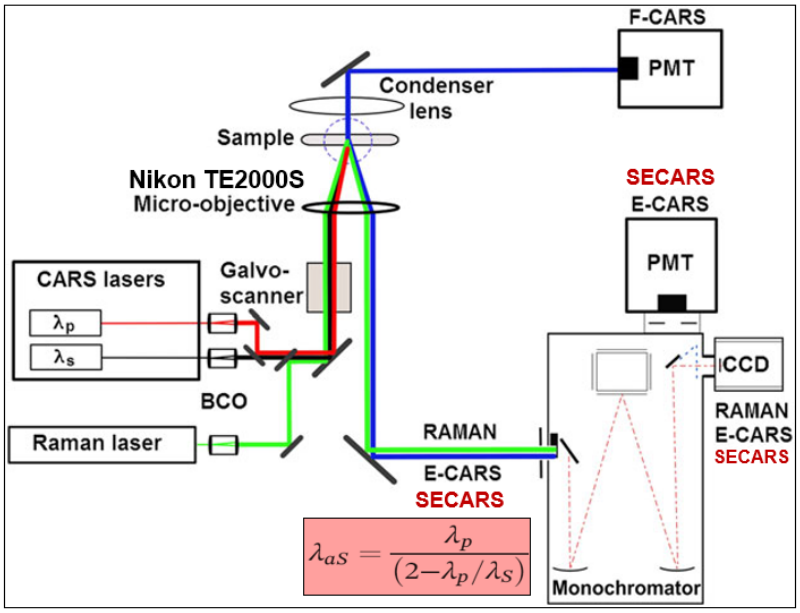

Fig.15. Schematic of the scanning laser microspectrometer "CARS"

For CARS microscopy, we use a water-immersion objective lens with a high numerical aperture (NA=1.2, UPLANAPO-60x, Olympus) to focus the beams tightly. With the tight foci, the phase-matching conditions are relaxed because of the large cone of wave vectors of the excitation beams and the short interaction length.

Signal mapping was performed during the laser beam focal spot 2D scanning by galvo-driven mirrors and recording at each spatial point the spectrum of Raman scattered radiation with both coherent and incoherent contributions. The galvo-scanner moves the focal spot across the selected sample surface area by the steps of about 0.5–1 μ (or more). In each spatial point, the spectrum is accumulated by the CCD array during the preset exposure time, typically ≈ 0.5–1s. Then, the spatial distribution of the power scattered into a preset spectral interval can be calculated. This matrix is presented as a microimage, or a map, of a signal strength. In case of the resonant signals, the signal strength is derived as the corresponding line amplitude above the level of the nonresonant background radiation.

SERS excited by 785-nm 85-MHz repetition rate 6-ps laser pulses

The results of SERS experiments with the picosecond-pulse excitation source related to the sample damage threshold estimation are presented in Figure 16. Here, one of the 1,338 cm^{-1} TNB line SERS maps, recorded at pump radiation at 785-nm wavelength, is presented (Figure 16a). This 12 μ × 12 μ map was obtained at the lowest, 0.085 mW average power at the surface within the laser spot diameter of about ~1μm. The 1,338 cm^{-1} TNB line strength span in Figure 16a is from ~70 (black) to ~1,100 (white) CCD analog-to-digital converter counts (the background signal is subtracted).

The graphs illustrating SERS signal strength variation with the average excitation power in some particular pixels of the map in Figure 16a are presented in Figure 16b. For comparison, the pixels with the smallest, intermediate, and largest SERS signal levels at the lowest power have been selected.

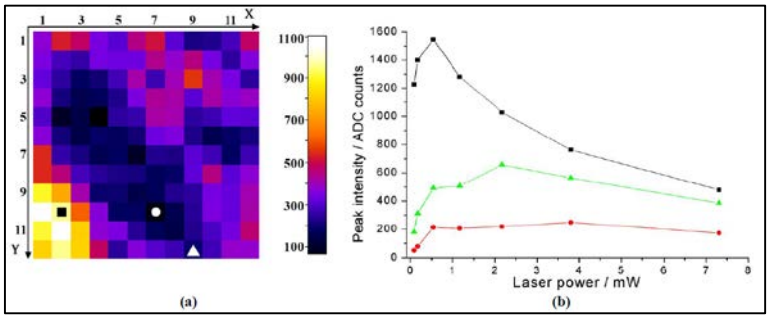

Fig. 16. (a) The 1,338-cm^{-1} TNB line SERS map of a 12-μ × 12-μ (1 μ spatial resolution, 1s exposure time) surface area at 0.085 mW average power of 785-nm excitation and (b) SERS signal strength variation versus average excitation power in three different pixels of the map: X = 2, Y = 10 (▪), X = 7, Y = 10 (•), and X = 9, Y = 12 (▲). The symbols on the map show the correspondence between the selected pixels and the data graphs in Fig. 16b.

It is clearly seen from the Fig.16 that the slopes of the signal growth in these pixels also differ from each other within an order of magnitude. Most probably this is due to different Raman signal enhancement provided by various Au-NP structures present within the laser spot. Thus, SERS signal strength dependences presented in Figure 16b show that the average excitation power should be kept well below 0.5 mW.

SECARS excited by 85 MHz repetition rate 6-ps laser pulses

Sample surface optical damage in picosecond-pump SECARS experiments was investigated using the 1,338 cm^{-1} TNB Raman line resonant pump laser beams at λ_p = 931 nm and λ_S = 1,064 nm provided by our CARS system. The obtained results shows that after one mapping scan even at moderate pump laser intensities the Au-NPs/CeO_2 active surface can be severely destroyed in the entire scan region. At the lowest powers used, the overall pattern is reasonably well reproduced when sequential mapping scans are performed at the same level of laser powers.

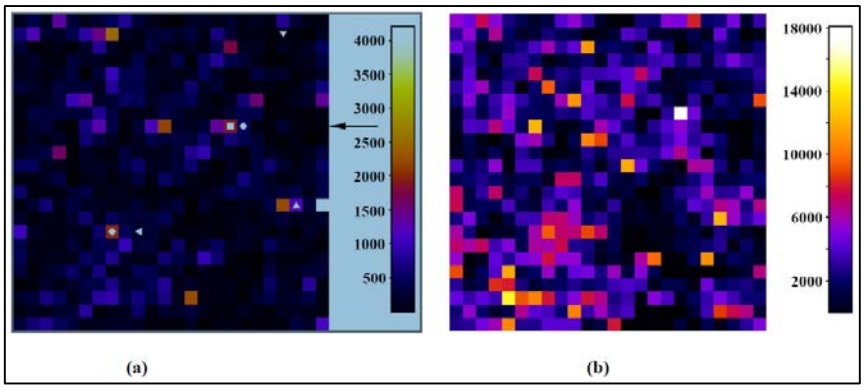

Fig. 17. The 1,338 cm^{-1} TNB line SECARS maps of the same 24 μm × 24 μm surface area of a sample (1 μ spatial resolution, 1s exposure time) at two different levels of laser powers: (a) P_p = 70μW, P_S = 125 μW and (b) P_p = 300 μW, P_S = 534 μW; λ_p = 931 nm, λ_S = 1,064 nm, and λ_{aS} = 828 nm.

The reproducible SECARS signal map in Figure 17a represents an example of data obtained at the lowest levels of Raman-resonant excitation of Au NP-bound TNB molecules. Here, the bright

spots in the recorded SECARS images, with the average distances between the spots of the order of 5 μ, are assumed to correspond to the spatial distribution of TNB/Au-NP conjugates of various sizes. In this case, the Au-NP clusters and islands are supposed to enhance all or some of the electromagnetic fields with λ_p, λ_S, and λ_{aS}.

Our estimations suggest that for our particular samples and CARS Raman microspectrometer, average lasers powers (P_p +P_S), recommended for more or less nondestructive and reproducible measurements, should be kept below 0.4-0.5 mW (corresponding to intensities 0.4–0.5 mW/μm^2), which is consistent with the results of our SERS measurements presented previously.

Thus, the intensity limits for CW or quasi-CW ps-pulse laser beams, employed in SERS or SECARS detection of Au-NP-bound TNB reporter molecules, were experimentally evaluated. For 85-MHz repetition rate sequence of 6-ps laser pulses in the range of 785-1,064 nm, the average threshold intensity was evaluated to be less than 0.5 mW/μm^2, which corresponds to a peak intensity of 1,000 mW/μm^2. The results of the experiments demonstrate that extreme care should be taken about the laser power employed while using SERS-active structures for analytical purposes in linear or nonlinear Raman experiments.

However, the experiments also showed that at Raman resonant two-color laser excitation of the reporter molecules strong enough SECARS signals can be generated at laser powers that do not destroy the organic-metal conjugates, and the sensitivity of SECARS measurements still remains rather high.

The high chemical imaging contrast demonstrated by the recorded SECARS microimages of Au NPs/CeO_2/Al/Al_2O_3 sample surfaces is promising in terms of reaching high SECARS detectability of the probed reporter molecules, as well as investigating the mechanisms of SECARS signal generation in further experiments.

2.1.5 Synthesis of core-shell nanostructures $NaYF_4$:Yb^{3+},Er^{3+},Tm^{3+}@SiO_2: bioimaging and tests in biomedicine.

The present report highlights our results on synthesis of $NaYF_4$:Yb,Er@SiO_2@Ag core–shell nanoparticles (CSNPs) for plasmon-enhanced upconversion luminescence (UCL) and preliminary bioimaging tests with neutrophil cells and biomedical tests with fibroblast cells. Hydrophilic surface UCL nanoparticles as cores were obtained by precipitation of Rare Earth Elements (REE) chlorides from water-alcohol solutions. The formation of a hydrophobic surface of α-$NaYF_4$:Yb,Er NPs was achieved by thermolysis method at 280 °C and β-$NaYF_4$:Yb,Er by precipitation method in nonpolar medium at 320 °C. Silica shell was formed by the modified Stöber method on the surfaces of UCLNPs with different polarity and phase composition. A mixture of hexane-cyclohexane-isopropyl alcohol was used as a medium for the formation of mononuclear CSNPs on hydrophobic surfaces of cores with different thicknesses of the silica shell: 5 nm and 14 nm (Fig. 18).

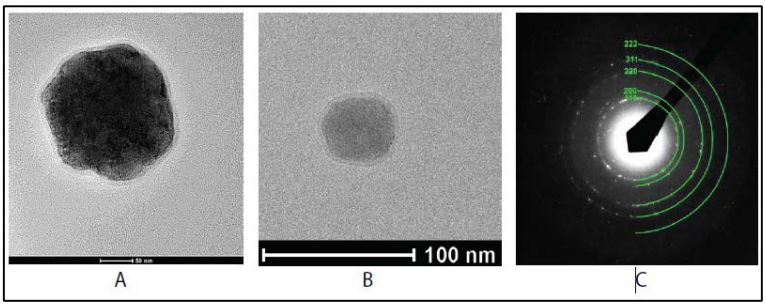

Fig. 18. TEM images of $NaYF_4$:Yb,Er@SiO_2 CSNPs with various core sizes: A) ~ 200 nm, B) ~ 45 nm and shell thicknesses of 5 nm, C) selected area electron diffraction (SAED) pattern.

To enhance the luminescence properties of the synthesized CSNPs we have proposed the direct embedding of AgNPs into the SiO_2 shell in parallel to its formation which eliminates the multi-stage synthesis. A colloidal solution of AgNPs was added to a mixture of hexanecyclohexane-isopropyl alcohol followed by the formation of a SiO2 shell. As a result of AgNPs embedding to our core-shell structure the UCL yield was enhanced for 85 and 29 times for structures with a shell thickness of 5 nm and 14 nm, respectively (Figure 19 a,b).

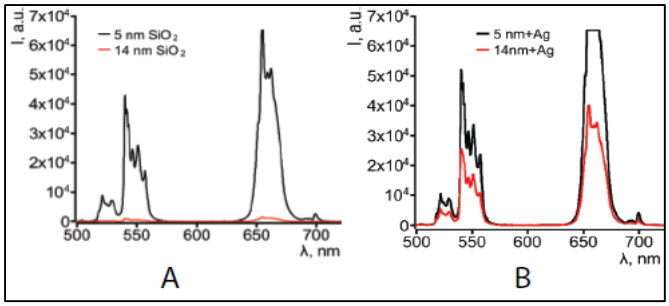

Fig. 19. UCL spectra of CSNP A) $NaYF_4$:Yb,Er@SiO_2 and B) $NaYF_4$:Yb,Er@SiO_2@Ag with two different thicknesses of SiO_2 shell: 5nm and 14 nm

We probed tests on UCL bioimaging of neutrophil cells. Neutrophil cells were immersed in saline with $NaYF_4$:Yb,Er@SiO_2@Ag CSNPs for 30 minutes to capture some quantity of phosphor NPs. Next, neutrophils were deposited on a microscope coverslip and fixed with an alcohol solution twice washed with distilled water and drying at room temperature. Figure 20 shows UCL image of neutrophil cell taken at the red band of the luminescence spectrum.

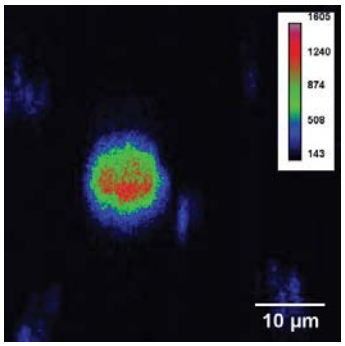

Fig. 20. UCL image of neutrophil cells.

Thereby, the first bioimaging test of synthesized core-shell nanoparticles as intracellular phosphors, showed the possibility of obtaining contrast bioimaging using neutrophil cells as an example.

We also probed these nanoparticles in our first tests on photodynamic therapy (PDT) using fibroblast cells as target cells and chlorophyll as a photosensitizer. The results of measuring the cytotoxicity of fibroblast cells before and after irradiation with a laser are presented below in table 1.

Table 1.

Staining with trypan dye assay			
№	Sample name	Negative control (without laser radiation)	Positive control (with laser radiation)
1.	Cells (fibroblasts)	92 ± 3 %	90 ± 5 %
2.	Cells + CS NPs (C=200ppm)	90 ± 4 %	87 ± 4 %
3.	Cells + CS NPs (C=200ppm) combined with Chlorophyll	**94 ± 3 %**	**69 ± 5 %**

The preliminary result on the number of fibroblast death cells (~25%) in PDT seems to be encouraging, though requires further optimization of this process.

3. Student program

1) **2018 – 2020**: 3 students – defense of master's degree

2) **2018 – 2019**: 2 students – defense of bachelor's theses

3) **2018 – 2019**: JINR UC Summer School, 2 students, Serbia and Egypt

4) **2018 – 2020:** Student summer practice program, 6 students

4. International cooperation, grants supported by Plenipotentiaries and FLNP prize:

Cooperation with:

Armenia, Belarus, Bulgaria, Cuba, Egypt, Uzbekistan, Latvia, Poland, Russia, Romania, Slovak Republic, Ukraine.

Grants supported by Plenipotentiaries:

Bulgaria, Poland, Romania, Slovak Republic

Number of publications (2018-2020) – 15 (17-18), expected by the end of 2020)
Number of conferences (2018-2020) – 21

The first FLNP prize for 2019 in the section "Experimental work"

Main publications

1. Arzumanyan G.M., Mamatkulov K.Z., Fabelinsky V.I., et al., “Surface-enhanced micro-CARS mapping of a nanostructured cerium dioxide/aluminum film surface with gold nanoparticle-bound organic molecules”, JRS, 49, **2018**, 7(2), pp. 1145-1154.

2. Poimanova O.Yu., Radio S.V., Arzumanyan G.M., et al., “Hexakis(dimethylsulfoxide-O)-cobalt(II) hexatungstate, [Co(C2H6OS)6][W6O19]: synthesis from aqueous di ethylsulfoxide solution, crystal structure determination, FT-IR and Raman spectroscopy analysis, and surface micromorphology”, J. Coord. Chem., 71(3), **2018**, pp. 1-19.

3. Sarychev A.K., Arzumanyan G.M., Mamatkulov K.Z., et al., “Optical properties of mesoscopic, multiscale silver films: surface plasmon localization and giant SERS”, Proceedings of SPIE-**2018**, Paper No.: OP101-87

4. Пойманова Е.Ю., Медведь А.О., Арзуманян Г.М. и др., «Декавольфрамат никеля [Ni(C2H6SO)5(H2O)]2[W10O32]: синтез из водно-диметилсульфоксидного раствора, определение кристаллической структуры, ИК- и КР-спектроскопический анализ, микроморфология поверхности», Ж. структ. химии, 59(1), **2018,** с. 149-157.

5. Арзуманян Г.М., А.В. Мудрый, О.С. Дымшиц и др., «Фотолюминесценция и структурные характеристики стеклокерамики, содержащей нанокристаллы оксида цинка и ионы европия», Труды конференции ФТТ-2018, 24-28 сент. **2018**, Т.2, с.254-257

6. Арзуманян Г.М., Линник Д.С., Маматкулов К.З., Глазунова В.С., «Синтез ап-конверсионных наночастиц SrF_2:Yb,Er@SrF_2», Труды III межд. конф. «Донецкие чтения-2018», 25 окт. **2018,** Т.2, с. 122-124

7. Arzumanyan G.M., Mamatkulov K.Z., Fabelinsky V.I., et al., “Laser intensity limits in surface-enhanced linear and nonlinear Raman micro-spectroscopy of organic molecule/ Au-nanoparticle conjugates”, JRS, **2019**; 50, pp 1311–1320.

8. Arzumanyan G.M., Linnik D.S., Mamatkulov K.Z., Vorobeva M.Yu., et al., “Synthesis of NaYF4:Yb,Er@SiO2@Ag core-shell nanoparticles for plasmon-enhanced upconversion luminescence in bio-applications”, Annals of Biomedical Science and Engineering, **2019**, 3, pp 013-019.

9. Zavatski Sergey, Khinevich Nadia, Arzumanyan Grigory, Bandarenka Hanna et al., “Surface Enhanced Raman Spectroscopy of Lactoferrin Adsorbed on Silvered Porous Silicon Covered with Graphene”, Biosensors, **2019**, 9, 34, pp. 1-19.

10. Арзуманян Г.М., Марченко А.С., Маматкулов К.З., Врещагин К.А., Волкоа А.Ю., "К вопросу о спектральной идентификации активированных и не активированных нейтрофилов методом комбинационного рассеяния света". Труды 61-ой Всероссийской научной конференции МФТИ, Москва, **2019**, стр. 27-28.

11. Arzumanyan G.M., Mamatkulov K.Z., Fabelinsky V.I., et al., “Micro-SECARS Studies of Organic Molecules on Randomly -Nanostructured SERS-Active Surfaces”, Proceedings of the 18-th European conference on non-linear optical spectroscopy (ECONOS), **2019**, April 7-10, Rouen, France, p.74, (Microspectrometer “CARS”).

12. Yakimchuk D.V., Kaniukov E.Yu., Arzumanyan G.M., et al., "Self-organized spatially separated silver 3D dendrites as efficient plasmonic nanostructures for Surface-enhanced Raman spectroscopy applications", J. Appl. Phys, **2019**, 126

13. Arzumanyan G.M., Gur'ev A.S., Mamatkulov K.Z., et al. "Micro Raman spectroscopy for NETosis detection”, JRS, **2020**, 1-10

Conferences

1. Арзуманян Г.М., «Поверхностно-усиленное микро-КАРС картирование органических молекул», Российская конференция и школа молодых ученых по актуальным проблемам спектроскопии комбинационного рассеяния света: «КР – 90 лет исследований», 28 мая – 01 июня **2018 г**., г. Новосибирск, Россия. **Keynote report**
2. Arzumanyan G.M., **"**Polarization-sensitive CARS imaging and surface-enhanced micro-CARS of organic molecules", BIT's 2nd International Biotechnology Congress-2018, October 14-16, **2018,** Fukuoka, Japan. Oral report.
3. Doroshkevich N.V.,"Detection of DNA molecules by SERS spectroscopy with silver porous silicon as an active substrate", International Conference on Analytical and Nanoanalytical Methods for Biomedical and Environmental Sciences: "IC-ANMBES 2018", 23-25 May, **2018,** Brasov, Romania.
4. Sarychev A.K., Arzumanyan G.M., Mamatkulov K.Z., et al., "Optical properties of mesoscopic, multiscale silver films: surface plasmon localization and giant SERS", Int. conf. SPIE-2018, 19-23 August, **2018,** San Diego, California, United States. Oral report.
5. Мудрый А.В., Арзуманян Г.М., «Фотолюминесценция и структурные характеристики стеклокерамики, содержащей нанокристаллы оксида цинка и ионы европия». VIII международная научная конференция ФТТ-2018, 24 – 28 сентября **2018**г., Минск, Беларусь, Oral report
6. Bandarenka H.V., Arzumanyan G.M., Mamatkulov k.Z., et al., "Comparison of SERS-activity of Silver Dendrites and Nanoparticles on Structured Silicon", Advanced Photonics Congress, 02 – 05 July, **2018,** Oral report.
7. Арзуманян Г.М., «Спектрально-структурные характеристики стеклокерамики на основе нанокристаллов ZnO и активированных редкоземельных элементов», Всероссийская научно-практическая конференция гос. Университета «ДУБНА», 21 – 23 ноября, **2018,** Дубна, Россия. **Plenary report**.
8. Arzumanyan G.M., Mamatkulov K.Z., Fabelinsky V.I., "Polarization-sensitive CARS imaging and surface-enhanced micro-CARS of organic molecules", First International Conference on Molecular Modeling and Spectroscopy, **2019**, 19-22 February, Cairo, Egypt. **Keynote report**
9. Arzumanyan G.M., Mamatkulov K.Z., Fabelinsky V.I., "Coherent surface-enhanced raman scattering: chemical imaging and intensity limits", EuroSciCon Conference on Nanotechnology and Smart Materials, **2019,** 08-10 July, Prague, Czech Republic. **Keynote report**
10. Arzumanyan G.M., "Modern Trends in Raman Microspectroscopy", International School of Nuclear Physics «JINR Days in Bulgaria», **2019,** 13 -17 May, Borovets, Bulgaria. **Oral report**
11. Mamatkulov K.Zh, Vorobeva M.Ju., Bandarenko H.V., Arzumanyan G.M. "Surface Enhanced Raman Spectroscopy of Organic Molecules Adsorbed on Silvered Porous Silicon Covered with Graphene", 4th International Conference on Nanotechnologies and Biomedical Engineering, ICNBME-2019, September 18-21, **2019,** Chisinau, Moldova. **Oral report**
12. Vereshchagin K.A. Volkov A.Yu., Gurev A.S., Kravtsunova D.E., Mamatkulov k.Zh., Marchenko A.S., Arzumanyan G.M., "Peculiarities of Micro Raman Spectra of Blood Neutrophils Transformed during NETosis as a Possible Marker of Sepsis Mortality", 18-th European conference on non-linear optical spectroscopy (ECONOS), **2019,** 7-10 April, Rouen, France. **Oral report**
13. Рудных С.К., Воробьева М.Ю., Маматкулов К.З., Арзуманян Г.М., "Структурно-функциональные особенности и колебательная спектроскопия фосфолипидов", «Площадка открытых коммуникаций» - Openbio-2019, Новосибирская область, наукоград Кольцово, 22-25 октября, **2019 г. Oral report**
14. Bandarenka Hanna, Khinevich Nadia, Zavatski Sergey, Mamatkulov kahramon, Vorobyeva Maria and Grigory Arzumanyan, "Study of proteomic analytes by surface enhanced Raman spectroscopy", VI International Caparica Conference on Analytical Proteomics **2019,** 08 – 11 July 2019, Caparica, Portugal. **Oral report**
15. Марченко А.С., Арзуманян Г.М., «Способы активации и микроспектроскопия нейтрофилов», 26-ая научно-практическая конференция студентов, аспирантов и молодых специалистов государственного университета «Дубна», г. Дубна, 18-19 апреля **2019 г. Oral report**
16. Marchenko A.S., Vereshchagin K.A., Volkov A.Yu., Mamatkulov K.Zh., Arzumanyan G.M., "Raman spectroscopy of NETosis: search for spectral biomarker", International Conference on Radiation Applications (RAP 2019), September 16-19, **2019,** Serbia, Belgrade. **poster**
17. Vorobeva M.Yu., Mamatkulov K.Zh., Bandarenka H.V., Arzumanyan G.M., "Highly Sensitive Surface-enhanced Raman scattering based on Silver Dendritic Nanostructures", EuroSciCon Conference on Nanotechnology and Smart Materials, **2019,** 08-10 July, Prague, Czech Republic, **Oral report**
18. Arzumanyan G.M., Bandarenko A.V., Mamatkulov K.Zh., "Ultrasensitive detection of analyte molecules at attomolar concentration by Raman spectroscopy", **2020,** Feb. 21-22, EuroSciCon-2020, Amsterdam, Netherlands, **Keynote report**